POLITECNICO DI TORINO
Repository ISTITUZIONALE

3D Modeling of Highway Guardrails for Sight Distance Assessment

Terms of use:

(Article begins on next page)

19 April 2024

3D modelling of highway guardrails for sight distance assessment

Alessandra Lioi, MSc

PhD candidate

Department of Environment, Land and Infrastructure Engineering, Politecnico di Torino

ORCID: 0000-0003-0812-4094

César De Santos-Berbel, PhD

Assistant Professor

Departamento de Estructuras y Física de Edificación, Universidad Politécnica de Madrid

ORCID: 0000-0001-9686-8872

Marco Bassani, PhD

Associate Professor

Department of Environment, Land and Infrastructure Engineering, Politecnico di Torino

ORCID: 0000-0003-2560-1497

Maria Castro, PhD

Associate Professor

Departamento de Ingeniería del Transporte, Territorio y Urbanismo, Universidad Politécnica de Madrid

ORCID: 0000-0001-8941-5795

26   **Abstract**

27   Safety barriers limit the severe consequences to occupants of vehicles leaving the roadway from

28   colliding with obstacles, yet they may significantly reduce the available sight distance (*ASD*). A

29   procedure was devised to accurately recreate highway guardrails in three dimensions (3D), fitting the

30   barriers onto the curve roadsides. The effect of these devices on the reduction of the *ASD* was thus

31   evaluated in a set of case studies comprising different curve radii overlapped with different vertical

32   alignments and combined each with two safety barriers in two-lane rural roads. The 3D models of

33   highway curves with the selected guardrails were created in a Geographic Information System. Then,

34   a geoprocessing model was used to compute the *ASD*. The results made possible to quantify the *ASD*

35   reduction produced by the barrier with higher containment level in relation to the highway design

36   parameters, which can assist authorities in developing more comprehensive safety device standards.

37

38   **Keywords**

39   Guardrails, Highways, Sight distance, Road safety, 3D modelling

40 Introduction

41 Road restraint systems are safety devices aimed at protecting drivers and occupants from the

42 consequences of vehicle departure from the carriageway, absorbing the impact energy. Since they

43 contain out-of-control vehicles within the road, the even more serious consequences resulting from

44 an impact against roadside fixed objects or the vehicle rollover are avoided (AASHTO 2018).

45 Road restraint systems are installed along medians and roadsides, so they limit the driver's

46 ability to see the roadway ahead (Wang et al. 2017). Steinauer and Mayer (1999) observed that on

47 left-hand curves on German motorways crashes are more frequent than on the counterpart right-

48 hand curves due to the sight-distance reduction caused by the median barriers. The limitation of the

49 available sight distance (*ASD*) is often in contrast with the need to guarantee a sufficiently long visible

50 portion of the road ahead where to complete manoeuvres safely. As a result, road designers must

51 satisfy both needs adopting adequate barriers and geometric characteristics preserving a minimum

52 *ASD* from potential conflict points and/or obstacles along the driving path (AASHTO 2018; Ministerio

53 de Fomento 2016; Ministero delle Infrastrutture e dei Trasporti 2001). Sight distance is one of the

54 most important elements not only in the road design but also in the road management to the aim of

55 traffic safety (Castro et al. 2016). Montella (2001) advocated cost-benefit analyses to choose the most

56 appropriate traffic containment device in terms of safety performance. Consequently, given the

57 effects of safety barriers on the *ASD*, it must be included in such analyses (De Santos-Berbel et al.

58 2018).

59 The installation and performance requirements of safety barriers in European countries are

60 regulated by European and national standards. As stated by European standards (CEN 2002, CEN

61 2011a; b, CEN 2012), barriers are classified according to several containment levels, the entity of the

62 deflection of the system and classes of dissipated impact energy. However, each Member State

63 imposes different minimum requirements based on the road characteristics and operating traffic

64 conditions (Ministerio de Fomento 2009, 2014; Ministero delle Infrastrutture e dei Trasporti 2004).

65 Hence, in similar roads operating under similar traffic conditions, barriers of different characteristics

66   may be installed in the same European country, as well as among countries. In this sense, barriers that

67   oversize the minimum standard requirements may be selected in a precautionary way while

68   significantly altering sight-distance conditions.

69   The selection of roadside barriers for new construction or safety upgrading involves

70   contemplating the combined effect of highway geometrics with limited sight distance (AASHTO 2011).

71   Sarhan and Hassan (2012) investigated the effect of different concrete barriers on the *ASD* for the

72   stopping maneuver. Nevertheless, studies addressing the impact and consequences in terms of sight

73   distance of installing different guardrails, which have a more complex three-dimensional (3D) shape

74   than concrete barriers, have not been found in the literature. Furthermore, it has been evidenced that

75   small differences in accuracy of 3D road items might produce significant variations in the *ASD*

76   estimation (Bassani et al. 2019; Iglesias et al. 2019). As a consequence, the 3D modelling of road

77   barriers must be carried out with the highest accuracy and precision.

78   This research aims to devise an advanced procedure to accurately recreate highway sections

79   with guardrails in 3D. Moreover, the procedure was tested for evaluating the effect of two different

80   guardrails on the *ASD* on curves in relation to the highway design parameters.

81   The paper is divided into five sections. The introduction is followed by a review of the current

82   state of the art. A subsequent section outlines the procedure devised to recreate the guardrails and

83   describes the organization of the case studies. The next section summarizes and discusses the results

84   obtained from the study. Conclusions and brief considerations about future research are presented in

85   the last section.

86

87   Related works

88   The *ASD* is the maximum length of the road stretch ahead measured along the future path that the

89   driver can see in the presence of sight obstructions, i.e. elements of the roadway and/or the roadside

90   (Castro et al. 2016). **Figure 1** illustrates how the *ASD* is measured along the vehicle trajectory as the

91   distance between the farthest point visible (D, detected from the intersection between the line of

92   sight – LOS – and the trajectory itself) and the point of view (A). From the point of view A, straight

93   lines may be built to link target points along the future path (B, C, D, …G); lines AB, AC, …, and AG are

94   sight lines from the driver's eyes. Since the lines AE and AF intersect the sight obstruction (the HI

95   element), the driver cannot see the road stretch from E to F. Hence, he/she can only see the sections

96   from A to D and from G: the *ASD* is, therefore, the arc length from A to D.

97   For safety reasons, the *ASD* must be greater than the distance used to stop the vehicle before

98   hitting an unexpected object along the lane (i.e., the stopping sight distance, *SSD*). Consequently, the

99   *ASD* may be considered in the evaluation of safe speed limits. The comparison between *ASD* and *SSD*

100   allowed assessing the influence of sight distance on road safety. Ibrahim and Sayed (2011)

101   incorporated stochastic risk measures due to insufficient sight distance to a crash prediction model to

102   evaluate the potential impact of horizontal curve design on the collision frequency. By analysing top

103   crash-prone segments, Gargoum and El-Basyouny (2020) showed that the crash frequency is 2 to 3

104   times higher where the required *SSD* is not met.

105

106
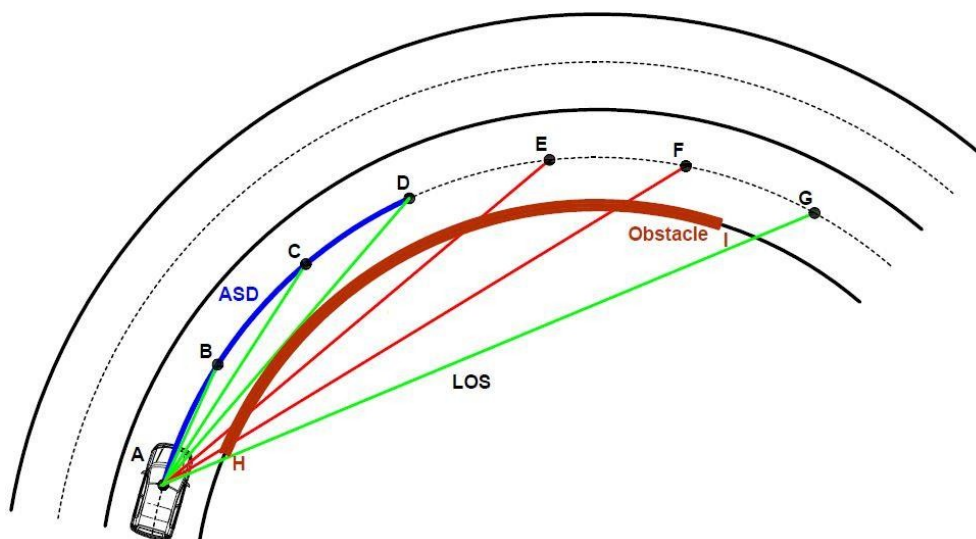
107   **Figure 1**. Graphical definition of the available sight distance (*ASD*).

108

109   For the *ASD* analysis, Spanish and Italian highway design standards (Ministerio de Fomento

110   2016; Ministero delle Infrastrutture e dei Trasporti 2001) provide values for the height of the driver's

5

111   eye and the height of a possible obstacle, with the driver's head position located at 1.1 m above the

112   pavement surface. Different obstacle heights are assumed in the assessment of *ASD* to check the

113   compliance with the *SSD* requirements: 0.1 m with the Italian standard, and 0.5 m with the Spanish

114   one. For research purposes, the heights of target may be differentiated from the standard values.

115   De Santos-Berbel and Castro (2018) set the driver's eye heights at 1.5 m and 2.0 m to simulate sight-

116   distance scenarios with heavy vehicles in the vicinity of underpasses, producing relevant variations in

117   the *ASD* outputs.

118   The *ASD* depends on cross-section elements, roadside features, and horizontal and vertical

119   alignment (Ismail and Sayed 2007). On existing roads, reduced sight distance may be caused by

120   inadequate geometric design, changes in the initial roadside conditions due to natural or human

121   actions, or both (De Santos-Berbel et al. 2013).

122   Although most current design policies contemplate the two-dimensional (2D) approach to

123   evaluate the *ASD*, the literature suggests that a 3D approach is much more reliable to avoid

124   overestimation or underestimation of the *ASD* (Castro et al. 2017). De Santos-Berbel et al. (2018)

125   studied and compared the differences between the output of 2D and 3D ASD analyses produced by

126   concrete barriers on curves on existing highways. The results found significant differences between

127   both procedures. Particularly, the superelevation, the effect of which could be included in the 3D

128   procedure, was found to affect the results. Papadimitriou et al. (2018) highlighted the need to consider

129   the combined effect of 3D alignments alloys and the presence of containment devices.

130   Many methods and algorithms have been developed and validated for the evaluation of the

131   *ASD*. Several authors have proposed *ASD* estimation procedures based on modelling the surface of

132   the roadway and roadside features to recreate the highway and its environment (Castro et al. 2014;

133   Ismail and Sayed 2007). Liu (2013) developed an analytical method to determine the available sight

134   distance on combinations of vertical and horizontal curves in the presence of roadside barriers. These

135   procedures have shown limitations to represent overhanging features in the road environment.

136   Alternatively, Campoy-Ungría (2015) suggested an *ASD* estimation method based on prismatic line-of-

137 sight buffers launched directly on a high-density LiDAR cloud of points, not requiring any terrain

138 surface. More recently, fully 3D methods have been developed and validated to obtain reliable *ASD*

139 results (Gargoum et al. 2018; Ma et al. 2018; De Santos-Berbel and Castro 2018).

140   Some recent investigations have been focused on the use of mobile laser scanning (MLS) data

141 to obtain point clouds to be used to accurately create 3D models of real driving scenarios along road

142 sections (Alcón Gil et al. 2021; Bassani et al. 2015; Ma et al. 2018; Shalkamy et al. 2020) and

143 intersections (Jung et al. 2018). The difficulties inherent in the use of MLS techniques stem, on the one

144 hand, from the strong dependence of the *ASD* analysis on the accuracy of the objects modelled in the

145 near environment and its modelling procedure to subsequently obtain realistic *ASD* values. Hence, a

146 dense cloud of points is required to enable a proper modelling of the shape of elements that may

147 represent a sight obstruction (Bassani et al. 2019; Iglesias et al. 2019). As a result, a significant amount

148 of data and storage capacity are necessary, with a significant share of data points that are not

149 effectively necessary for the analysis (i.e., inefficient). On the other hand, the use of MLS is, in

150 principle, limited to real scenarios and is not suitable to be used in road design scenarios.

151 Nevertheless, the procedure utilized in this study is capable of incorporating 3D features derived from

152 MLS surveys along with virtual new elements to recreate different scenarios (Alcón Gil et al. 2021; De

153 Santos-Berbel and Castro 2018).

154   To lighten the computational burden and related costs to carry out sight distance calculation,

155 Ma et al. (2019) have introduced the use of a convolutional neural network that enables the

156 estimation of the *ASD* using far fewer points. This algorithm improves the above reported

157 inefficiencies related to the use of large databases from MLS, partially solving the former of the two

158 issues abovementioned.

159   Spatial analysis and environment modelling capabilities of geographic information systems (GIS)

160 have led to the development of *ASD* estimation procedures (Khattak and Shamayleh 2005). Castro et

161 al. (2011) provided a 3D approach based on viewsheds to evaluate *ASD* by using GIS tools. Later on,

162 Castro et al. (2014) provided a more efficient procedure based on algorithms that iterated lines of

163 sight. Bassani et al. (2016, 2019) evaluated the *ASD* in an urban road scenario where several sight

164 obstruction types are present, intending to highlight and compare the computational efficiency,

165 advantages and drawbacks of GIS and numerical computing codes.

166 The use of a GIS in highway sight distance studies can help solve part of the difficulties in the

167 use of traditional design software because it can be employed to carry out other geometric and safety

168 analyses. For example, consistency and safety analyses are carried out overlapping with GIS the

169 information coming from crash counts, operating speeds, traffic data, road features, and geometric

170 characteristics of a highway (Castro and De Santos-Berbel 2015; Iglesias et al. 2016). Furthermore, the

171 detection of shortcomings and hidden dips in the 3D alignment can also be carried out in the GIS

172 environment (Castro et al. 2017; Castro and De Santos-Berbel 2015). Road design standards and

173 guides can be used in a GIS to generate realistic 3D road models starting from 2D data including

174 centreline and basic cross-sectional information (Wang et al. 2014). Current GIS applications are

175 robust enough to model road elements and obtaining results comparable to those coming from sight

176 inspections. Finally, GIS is a flexible tool that can also overcome the limitation of MLS based techniques

177 because it can easily include 3D sight obstructions, e.g. objects in the roadside like poles, installations,

178 and safety barriers.

179

180 Methodology and materials

181 This section outlines the procedure to build up the 3D model of the horizontal curves with the selected

182 guardrails for the assessment of the *ASD*. The computer software used to analyse the 3D models is

183 also described.

184

185 3D modelling: barrier design

186 The importance of accurately and precisely modelling the road and its environment in 3D, guardrails

187 included, stems from obtaining reliable results from the analysis. In this sense, these devices must be

188 accurately recreated and adapted to the roadside for any given highway alignment layout. The

8

189   assessment of the *ASD* contemplated two different types of guardrails. The first one is a 2-wave

190   N2-type guardrail, which reflects the guardrail typically installed on Spanish two-lane rural highways.

191   The second one is a 3-wave H2-type guardrail, widely used in Italy on the same road type. The process

192   devised to create the 3D barrier models is illustrated in **Figure 2**. All the relevant components of their

193   profile were drawn on computer-aided design software. It is worth noting that the considering

194   elements must be represented with closed lines to facilitate the operations in 3D drawing software

195   used later.

196   The cross-section drawings displayed in **Figure 3** were imported into SketchUp Pro to create the

197   3D models. Then, the barrier beam was extruded along a straight guideline perpendicular to the plane

198   containing the beam cross-section. This guideline, represented by the red dotted line in **Figure 4**,

199   serves in turn as the reference line for the installation of the barrier since it is located at the same

200   height as the base of the posts and in the same vertical position as the generating line of the beam

201   closest to the road centreline. Next, the barrier posts were replicated and inserted at the specified

202   fixed distances throughout the barrier (4 m for the N2 type, 2 m for the H2 type), thus obtaining the

203   3D model of the guardrails displayed in **Figure 4**.

204   The straight barrier displayed in **Figure 4** serves as a template to create the required barrier

205   models for any highway alignment. SketchUp Pro was selected to take advantage of the CLF Shape

206   Bender extension, which makes it possible to adapt a given shape, not necessarily with a

207   homogeneous cross-section, to a 3D curve given a guideline for the original shape and another

208   guideline for the target shape (Trimble 2013).

209
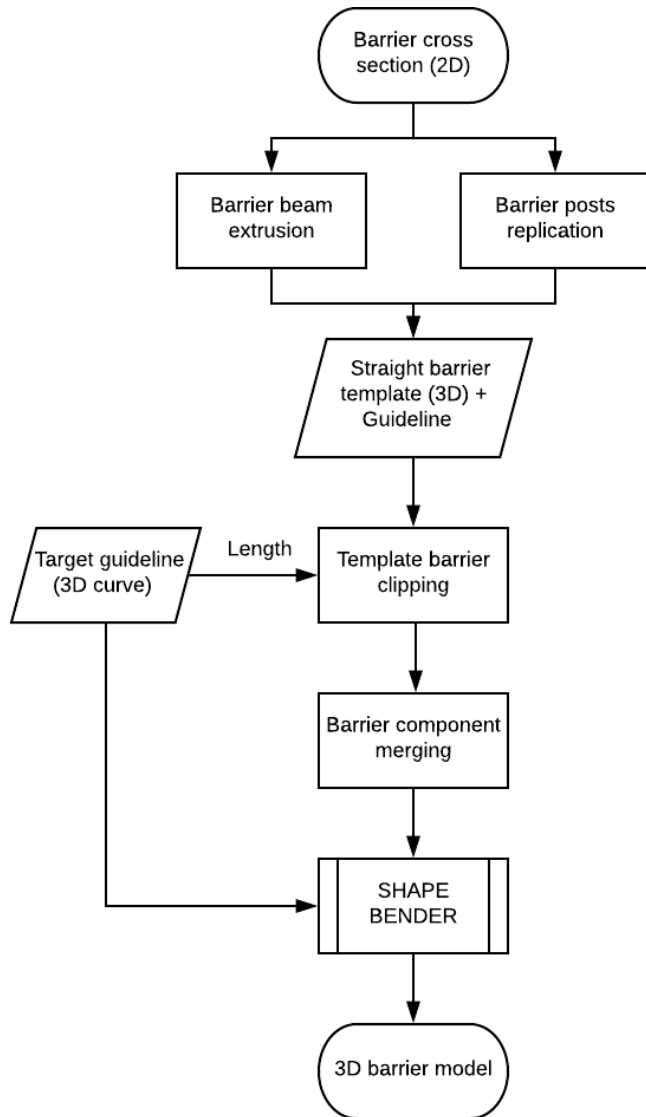
**Figure 2**. Flowchart of the 3D barrier model creation process.

211

212
213   (a)   (b)
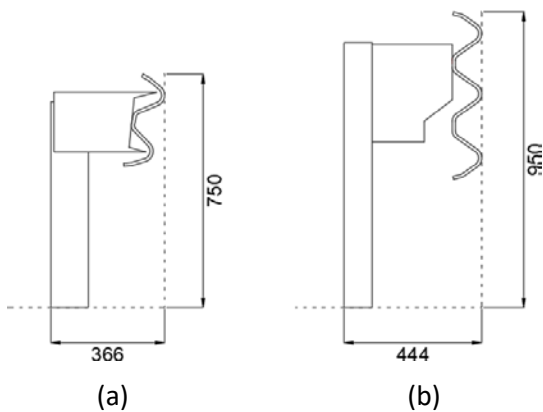
214   **Figure 3**. Cross-sections of N2 (a) and H2 (b) metallic barriers (unit of measurement: mm).
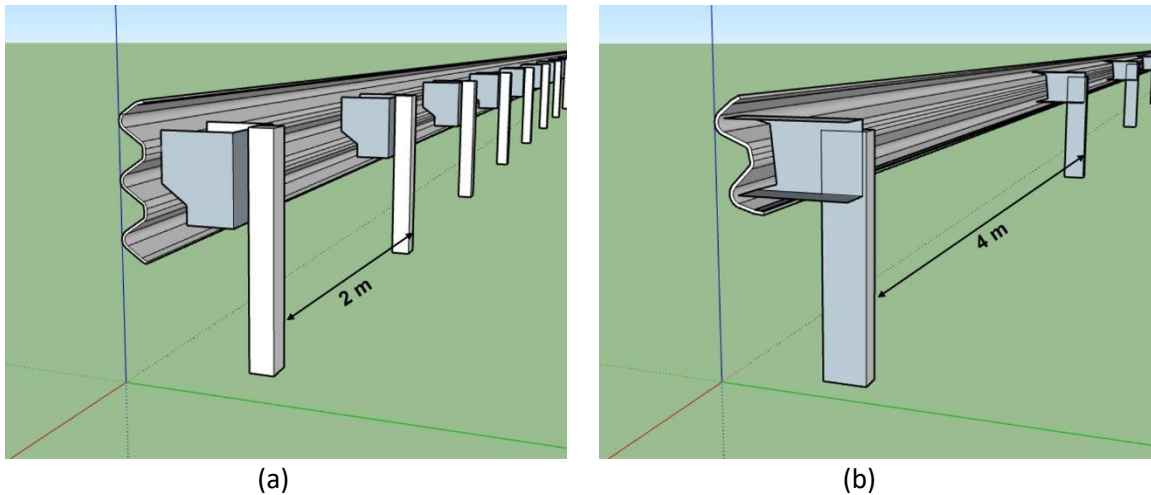
216 (a) (b)
217 **Figure 4**. 3D view of N2 (a) and H2 (b) selected guardrails in SketchUp Pro.

218

219 To create a barrier that suits the highway curve in 3D, the 3D curve featuring the roadway inner

220 edge was imported into SketchUp. Next, for producing a barrier without longitudinal distortion, the

221 straight barrier template and its guideline were clipped with length equal to that of the target

222 guideline. Then, all the resulting guardrail components were merged into a single object as required

223 to launch the Shape Bender extension. The 3D guardrail models thus produced were exported as

224 Collaborative Design Activity (COLLADA) format and then imported into a multipatch feature in

225 ArcScene (3D GIS environment), where they were placed in their final position (**Figure 5**). A multipatch

226 feature is a GIS entity whose specific data represent the outer surface of an object, which occupies a

227 volume in the 3D space (ESRI 2008).

228
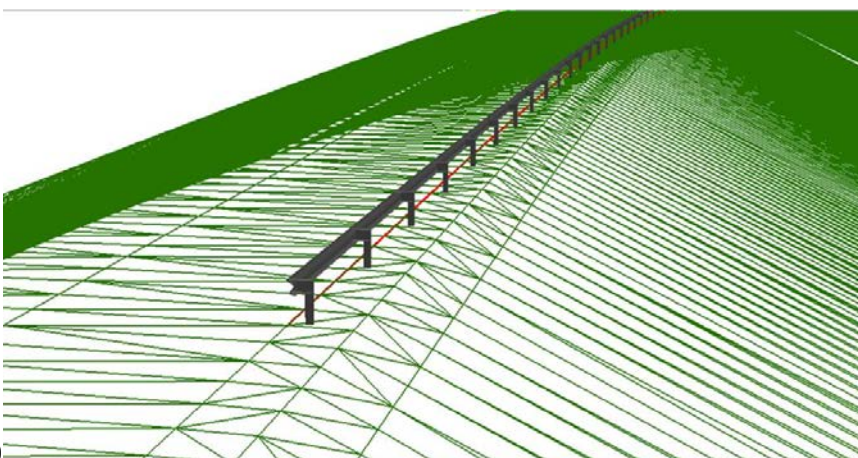
229
230 **Figure 5.** 3D view in ArcScene of N2 guardrail inserted on the TIN model and fitted to the roadside
231 (red line).

11

232 *Geoprocessing model*

233 Whereas the feature classes representing different types of barriers as visual obstructions that

234 comprise the 3D model were laid out in the 3D environment of ArcScene, the evaluation of the *ASD*

235 was run in ArcMap 10.3. This allowed boosting computation performance while maintaining the 3D

236 nature of the highway model. Numerical results were obtained by using a GIS geoprocessing model

237 developed and validated by the authors (Iglesias et al. 2016; De Santos-Berbel and Castro 2018). This

238 geoprocessing model is based on tools from the 3D Analyst extension of ArcMap and it permits to

239 consider 3D visual obstacles. First, "Construct sight lines", which connects the positions in space of the

240 driver's eye point and the target points (ESRI 2021a). Then a sequential automatic selection of the

241 generated line feature class input the "line of sight" tool along with the elevation model and the

242 multipatch feature class (ESRI 2021b). It evaluated whether each line of sight is obstructed by any of

243 the model features and, if so, returns a new point feature class containing the exact position in space

244 where the lines of sight were obstructed. In addition, the geoprocessing model outputs the sight

245 distance evaluation results from which the *ASD* values are retrieved.

246   The data required to execute this geoprocessing model includes the theoretical path followed

247 by a vehicle (with stations spaced 5 m apart) and the elevation model which recreates the highway

248 and its roadsides. In general, two types of elevation models are available: digital terrain models (DTM)

249 and digital surface models (DSM). A DTM is a 3D representation of the terrain surface which includes

250 exclusively the elevation of the bare ground, without vegetation, traffic signs, or buildings. On the

251 other hand, DSMs consider the structures on the surface, also detecting overhanging features.

252 Nevertheless, when overhanging features are present by the roadsides (as in the case of safety

253 barriers), the intrinsic features of DSMs do not support two points on its surface having the same

254 horizontal projection and different elevation values (Iglesias et al. 2016; De Santos-Berbel and Castro

255 2018). To overcome this problem, the highway 3D model was built up combining a DTM and fully-3D

256 modelled landscape features. The former was built up in GIS from a cloud point created using CLIP

257 version 1.29 road design software (TOOL S.A. 2013). The point cloud was created from the most

258 relevant points of road cross-sections spaced 1 meter apart. Next, a triangular irregular network (TIN)

259 (surface defined by the mesh in **Figure 5**) was built considering the point cloud as the node set. The

260 later comprises the multipatch feature classes modelling the guardrail as a sight obstruction. The

261 procedure allows to include mass standardized constructive elements into the highway 3D model in

262 the GIS environment. Therefore, the method hereby presented provides reliable results thanks to the

263 incorporation of lifelike-modelled 3D objects.

264 It must be noted that guardrails do not constitute a simple continuous obstacle like vertical

265 surfaces (e.g., walls, rigid concrete barriers), but they might enable the driver to perceive the road

266 ahead through the spaces between posts beneath the barrier beam. In this sense, the capability of the

267 geoprocessing model to return the 3D position of the visual obstruction and identify the visual

268 obstacle that obstructed each line of sight made it possible to accurately assess the *ASD* in the

269 presence of guardrails contemplating its complex 3D shape.

270 Furthermore, the driver's eye height and the target height are two required input parameters

271 of the geoprocessing model. Their values were taken according to the Spanish highway design

272 standard, as 1.1 and 0.5 m, respectively (Ministerio de Fomento 2016).

273 The algorithm first launches sightlines connecting the driver's point of view and targets located

274 along the vehicle path ahead, up to a prespecified maximum distance. Next, it checks whether the

275 sightlines are obstructed or not by either the DTM or the inserted multipatch features and retrieves

276 the *ASD* values.

277

278 Experimental design

279 To test the procedure for building up 3D models, a set of highway alignments was created. Nine

280 horizontal curves were designed with different radius, each one connected to spirals at both ends.

281 Two alternative vertical profiles were designed for each curve: a flat-grade profile and a profile with

282 vertical curves overlapped to each horizontal curve according to the alignment coordination principles

283 (Ministerio de Fomento 2016; Ministero delle Infrastrutture e dei Trasporti 2001). The cross-section

284 consists of a 7-m wide travelled way with two lanes (3.50 m each), one per driving direction, and 0.5

285 m-wide shoulders. Since the guardrail was placed in such a way that the horizontal projection of the

286 innermost generatrix of the beam coincides with the outer edge of the shoulder, the lateral offset

287 with respect to the travelled way was 0.5 m. In terms of design speeds, radii, and superelevation of

288 curves, two categories of roads can be distinguished, the so-called *Group 2* and *Group 3* according to

289 the Spanish standard denomination for undivided highways (Ministerio de Fomento 2016).

290 The geometric features of the horizontal curves are provided in Table 1. The length of each

291 curve has been laid out to ensure that the ends of the lines of sight that determine the minimum *ASD*

292 associated to the curve lie within the bounds of the circular arc of the curve on both travelling

293 directions. Table 1 also includes the parameter K_V (equation 1) of the overlapped vertical curve.

294 Negative K_V values correspond to vertical crest curves while positive ones correspond to vertical sag

295 curves. Design speeds in *Group 2* range from 120 to 80 km/h at intervals of 10 km/h. In *Group 3*, design

296 speeds range from 80 to 50 km/h. The design speed values are associated to the minimum radius

297 allowed in a highway segment as indicated in Table 1.

298 $$Kv \ = \ 100 \cdot L/\theta$$ Eq. 1

299

300 where K_V is the vertical curve parameter in m, *L* is the length of vertical curves in m, and θ is the

301 absolute value of the algebraic difference between the outbound i_2 and inbound i_1 grades in %.

302 To carry out the sight-distance analysis using the geoprocessing model, either guardrail model

303 was set by the inner roadside of each curve. The *ASD* estimation was repeated for both travelling

304 directions.

305

306 **Table 1.** Geometric characteristics of the horizontal curves. The negative value of K_V indicates a crest
307 vertical curve (group 2), a positive value represents a sag vertical curve (group 3).

Group	Section	Horizontal radius (m)	Design speed (km/h)	K_V (m)	Superelevation (%)	SSD (m)
2	Curve 1	700	120	- 38467.98	8	261.49
	Curve 2	550	110	- 30218.00		216.79
	Curve 3	450	100	- 24718.02		178.59
	Curve 4	350	90	- 19218.05		145.48
	Curve 5	250	80	- 13718.10		116.85
3	Curve 6	265	80	+ 14617.94	7	116.85
	Curve 7	190	70	+ 9515.16		91.17
	Curve 8	130	60	+ 6750.37		69.67
	Curve 9	85	50	+ 4198.36		51.73

308

309 As previously stated, the *ASD* along a highway section must meet the distance needed for

310 vehicles to stop (i.e., *ASD* ≥ *SSD*). *SSD* is measured from the driver's position at the time when the

311 obstruction appears and justifies the braking. It includes two contributions: the distance covered by

312 the vehicle from the instant the driver perceives the obstacle to the instant the brake is applied (i.e.,

313 the perception and reaction distance) and the distance needed to stop from the instant the braking

314 maneuver begins (i.e., the braking distance). *SSD* in m is evaluated according to Equation 2:

315
$$SSD = \frac{V \cdot t}{3.6} + \frac{V^2}{254 \cdot (f_l + i)}$$
Eq. 2

316

317 where *V* is the design speed in km/h, *t* is the perception and reaction time (2 s, according to the

318 Spanish standard (Ministerio de Fomento 2016), f_l is the longitudinal friction coefficient (as a function

319 of the design speed), and *i* is the longitudinal grade in %. Table 1 provides *SSD* values for this

320 experiment. In this assessment, the longitudinal grade was neglected due to its small values. **Figure 6**

321 gives the flow chart of the sight distance analysis.

322
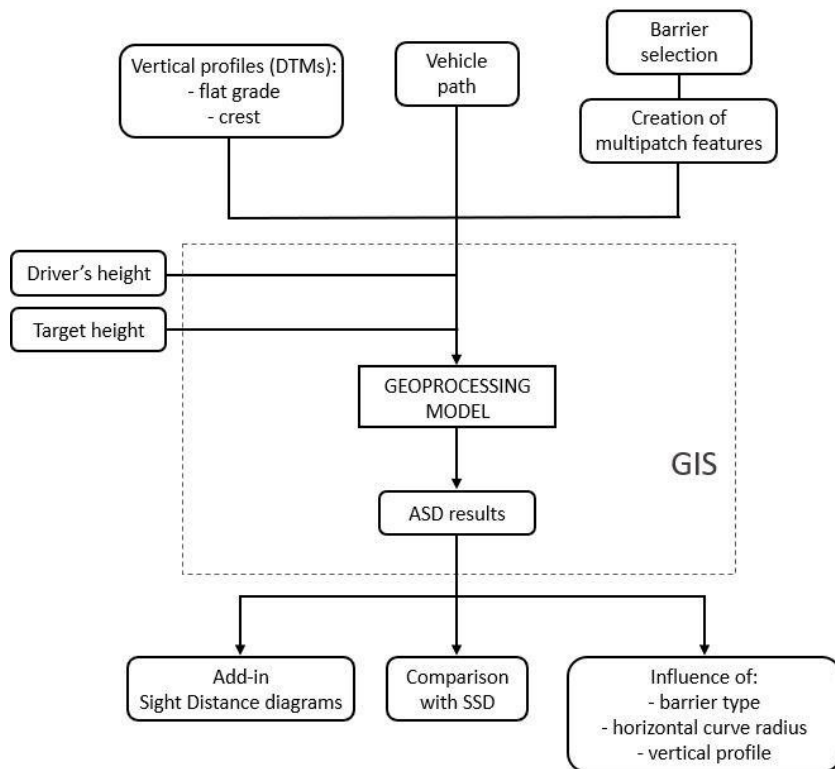
Figure 6. Flow chart of the research study.

By setting the vehicle trajectory and the roadside features, the geoprocessing model elaborated the sight distance diagrams with both profiles. Once the *ASD* values had been extracted, the impact of the barrier type on the *ASD* in function of the horizontal curve radius and the vertical profile was determined.

Results and discussion

The minimum ASD values obtained for each alignment on either travelling direction combined in turn with either guardrail model have been extracted. The aforementioned capability of the geoprocessing model to identify the position and the visual obstacle at which lines of sight are intercepted made it possible to assert that in the case studies the ASD limitation was produced by the barrier beam. Although lines of sight might pass through the gap between the barrier posts, it was checked that these lines did not affect the *ASD* output since the limiting feature was found to be the barrier beam in all cases.

16

339   First, horizontal curves overlapped with the flat-grade profile were analyzed with either barrier,

340   discerning between left-hand and right-hand curves (**Figure 7**). Considering that in the absence of

341   visual obstructions the *ASD* would be unlimited, a reduction of the *ASD* is observed in all the curves

342   due to the presence of barriers.

343   On left-hand curves overlapped with flat-grade profile (**Figure 7**a), the *ASD* is greater than the

344   required *SSD* in all group 3 curves (those with smaller radius) with both barrier types. A greater

345   decrease of the *ASD* with the H2 guardrail due to its higher size is evident. This reduction in *ASD*

346   increases as the radius of the curve increases too. For curves of Group 2, the *ASD* met the required

347   *SSD* in the presence of the 2-wave N2 barrier, except for the curve with *R* = 700 m (*ASD* = 260 m vs.

348   *SSD* = 216.8 m). The 3-wave H2 barrier does not allow the *ASD* to meet the required *SSD* in curves with

349   a larger radius (e.g. *ASD* = 210 m vs. *SSD* = 261.5 m for *R* = 700 m).

350   In right-hand curves (**Figure 7**b), barriers do not guarantee the required *SSD* in almost all the

351   analysed cases, with a greater obstruction given by the 3-wave H2 barrier. The greatest sight distance

352   deficits are observed for the largest radii: with the H2 barrier, the *ASD* values are lower than half of

353   the required *SSD* (e.g. *ASD* = 120 m vs. *SSD* = 261.5 m for *R* = 700 m). The N2 guardrail provides *ASD*

354   always larger than *SSD* only curves of smaller radius (e.g. group 3, *ASD* = 55 m vs. *SSD* = 51.7 m for

355   *R* = 85 m).

356   As expected, results depict that the installation of 2-waves guardrails is less unfavorable than

357   the installation of 3-waves ones in terms of sight distance. All else being equal, the *ASD* is greater in

358   left-hand bends, while in right-hand curves it is more difficult to guarantee it, especially in curves with

359   larger radii.

360   Since there are two different cases for vertical profiles (flat-grade and with vertical curves), it is

361   possible to compare the effect of the same barrier in different vertical alignments. Figure 8 shows the

362   analyses for N2 barrier, while Figure 9 those for H2 guardrail.

363   a)

364   b)
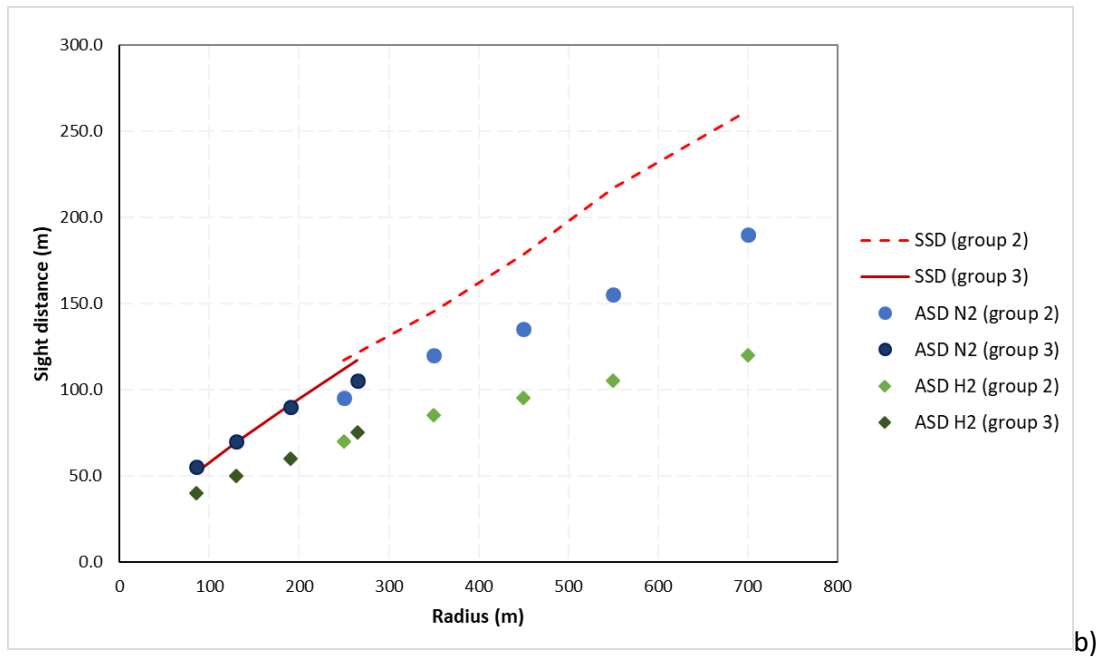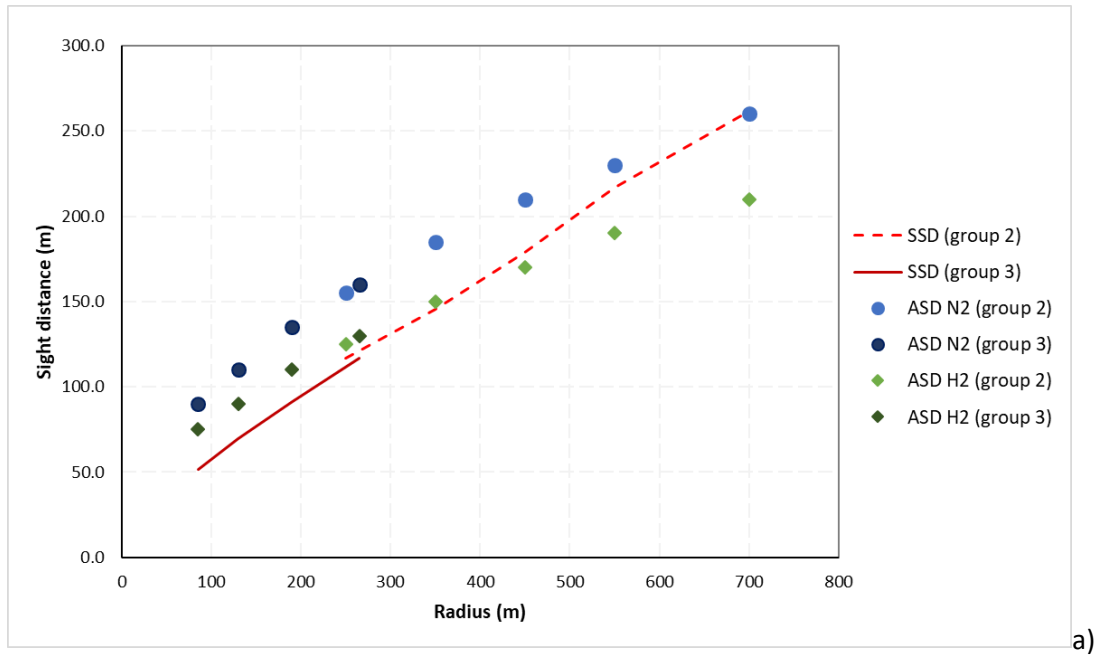
Figure 7. Sight distance analysis as a function of the radius on horizontal curves overlapped with flat grade: a) left-hand curves, b) right-hand curves.

Considering the N2 barrier in left-hand curves (Figure 8a), the *ASD* is greater than the required *SSD* in all group 3 curves for both types of vertical profiles (flat and sag). The greatest *ASD* values are reached in the non-flat profile, with sag vertical curves. For group 2 curves the *SSD* is always guaranteed in the flat-grade terrain. However, the vertical profile with crest curves does not allow the *ASD* to meet the required SSD in curves with a larger radius (e.g. *ASD* = 225 m vs. *SSD* = 261.5 m for *R* = 700 m).

18

374 a)

375 b)
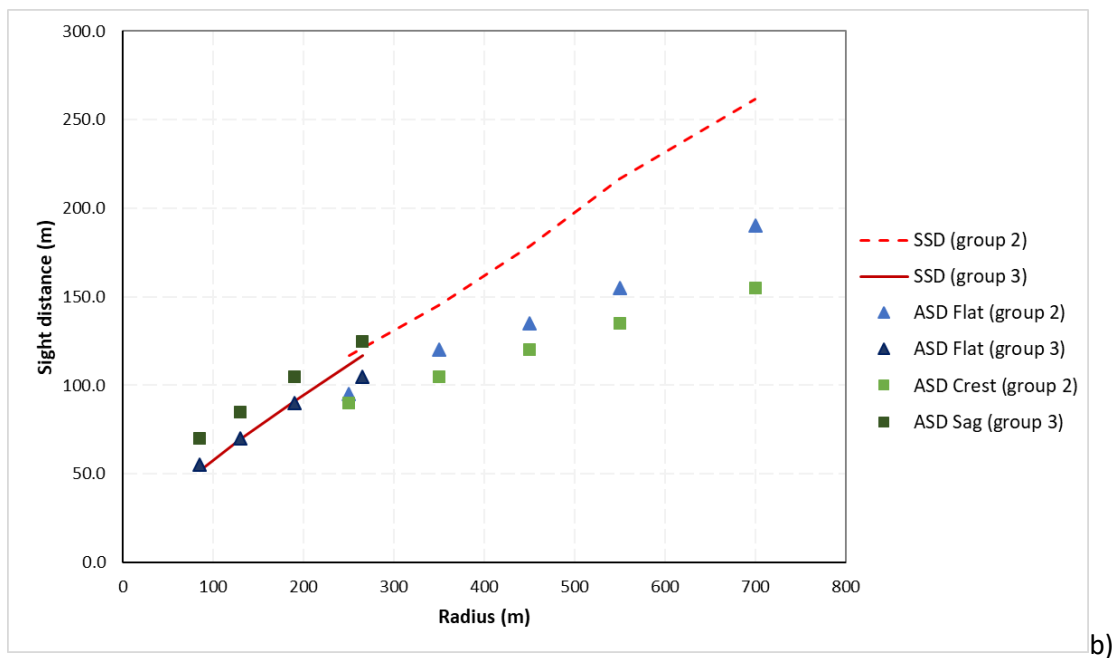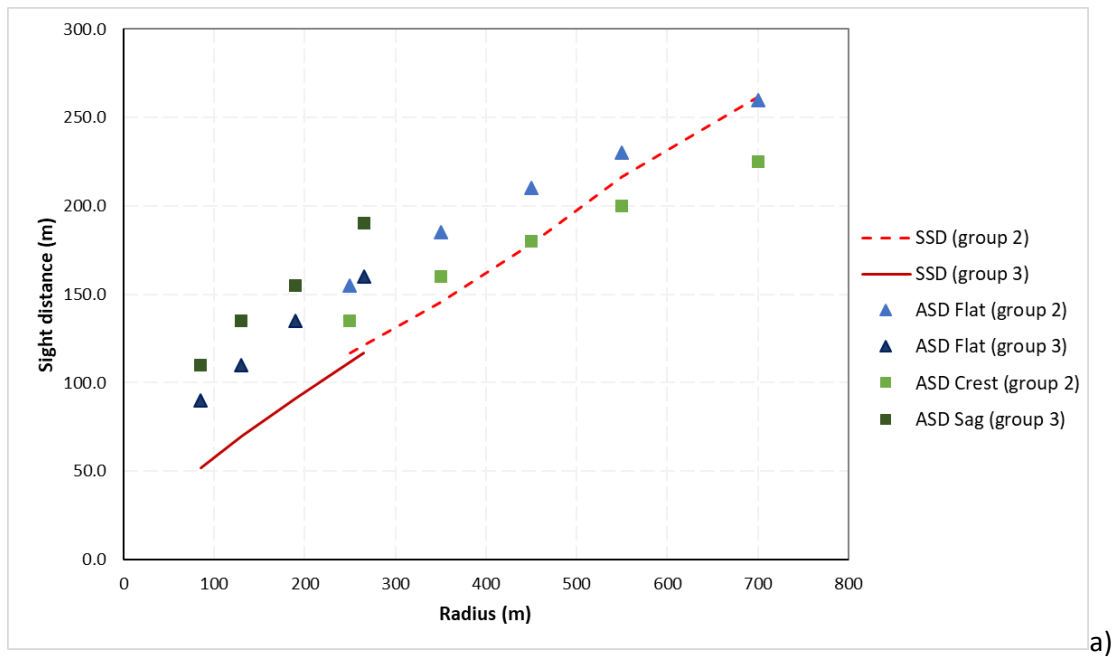
Figure 8. Sight distance analysis in function of the radius on horizontal curves overlapped with N2
barrier: a) left-hand curves, b) right-hand curves.

Even considering two different vertical profiles, the situation in terms of *ASD* is critical for

right-hand curves (Figure 8b). For group 3 curves, the sag vertical profile guarantees *ASD > SSD* in all

curves; *ASD* values are lower than the required *SSD* for the group 2 curves, with both vertical profiles,

especially with the flat-grade terrain.

By setting the H2 barrier in left-hand curves (Figure 9a), the *ASD* values exceeded the required

SSD in all group 3 curves with both types of vertical profiles (flat and sag). In this case, sag vertical

385   curves provide better sight conditions as well. A different situation occurs for group 2 curves, where

386   the *ASD* meets the required *SSD* just in the flat-grade terrain in the smallest curvature radii of the

387   category (e.g. *ASD* = 125 m vs. *SSD* = 116.8 m for *R* = 250 m). This trend is again justified by the vertical

388   profile: if the sag vertical curve provides a better sight distance, the crest one decreases the length of

389   the road visible from the driver point of view.

390   In right-hand curves (Figure 9b), sight conditions do not comply with safety requirements in the

391   presence of H2 guardrail, and the difference between *ASD* and *SSD* increases as the curve radius

392   increases. *ASD* values for the flat-grade terrain and crest curve vertical profile are almost identical; in

393   particular, in group 2, they coincide. This is attributable to the smaller distance between the driver

394   and the sight obstruction (i.e., the guardrail), with the result that the same sight line is obtained for

395   both cases (i.e., flat-grade and crest).

396   By analysing the *ASD* values for the two different vertical profiles, it can be observed that the

397   presence of vertical curves impacts the sight distance: *ASD* increases in presence of sag curves (from

398   *ASD*(N2) = 90 m and *ASD*(H2) = 75 m for "flat" profile to *ASD*(N2) = 110 m and *ASD*(H2) = 85 m for "sag"

399   profile, for *R* = 85 m, left-hand curve; from *ASD*(N2) = 110 m and *ASD*(H2) = 90 m for "flat" profile to

400   *ASD*(N2) = 135 m and *ASD*(H2) = 105 m for "sag" profile, for *R* = 130 m, left-hand-curve). Although

401   safety conditions are usually met in the left-hand curves, it is clear that crest vertical curves decrease

402   the *ASD* values (from *ASD*(N2) = 210 m and *ASD*(H2) = 170 m for "flat" profile to *ASD*(N2) = 180 m and

403   *ASD*(H2) = 155 m for "crest" profile, for *R* = 450 m, left-hand curve).

404   The results documented in this manuscript are consistent with those obtained by Sarhan and

405   Hassan (2012), where they found that crests provide reduced ASD values, while sags increase the ASD

406   in comparison to the flat-grade terrain case in the presence of concrete barriers. In particular, as the

407   absolute value of K_V decreases, *ASD* increases on sag curves and decreases on crests. Reduced lateral

408   offsets were also found to affect negatively sight distance conditions. In this sense, the research results

409   are also in line with preliminary results of the authors on existing highways in the presence of concrete

410   barriers (De Santos-Berbel et al. 2018).

411
a)

412
b)
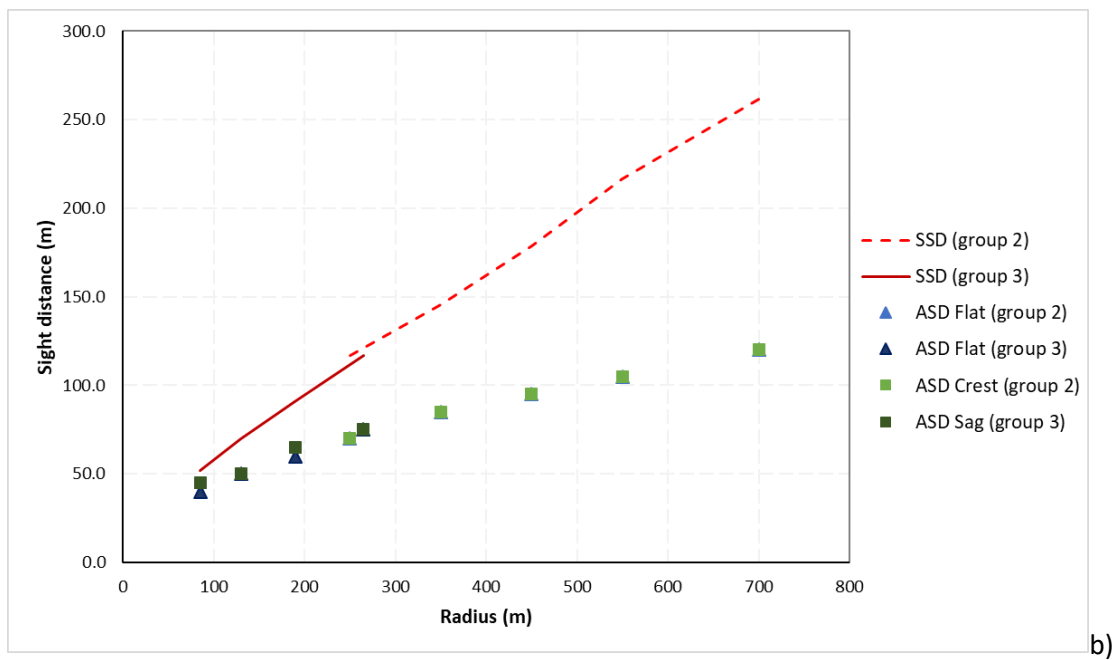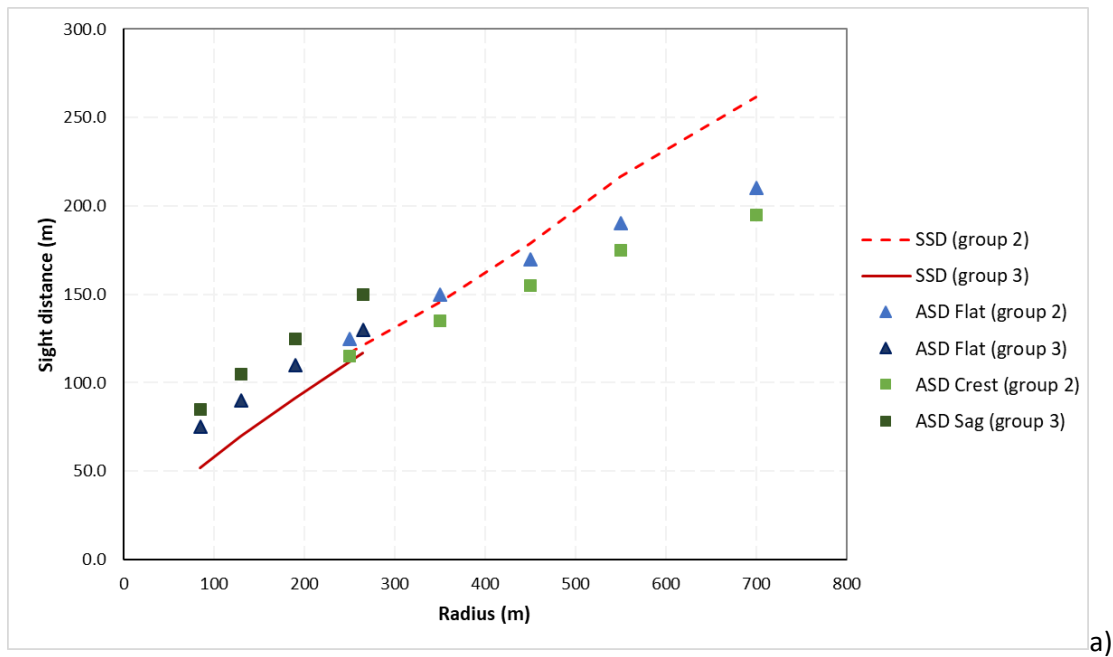
413 **Figure 9.** Sight distance analysis as a function of the horizontal radius on curves overlapped with H2
414 barrier: a) left-hand curves, b) right-hand curves.

415

Conclusions

Research contribution

418 Previous studies demonstrated that GIS is a useful tool to carry out sight distance analyses on 3D

419 models developed on existing road segments as well as on road projects. At present, no other

420 modelling technique can provide reliable and fast results on road design scenarios. This study intended

421   to assess the variations of *ASD* due to different safety barrier types (i.e., their height) which can result

422   from a difference in the design decision or cross-country difference in road standards. To this aim, the

423   Shape Bender extension in the SketchUp Pro 2019 environment was used to adapt barriers to terrain

424   models depicting different combinations of horizontal and vertical alignment. This tool greatly

425   facilitates the 3D design, and it is particularly useful for roads and infrastructures.

426   GIS tools are useful to understand the effects of two different guardrail models on the *ASD* in

427   curves. The use of multipatch features allows considering in the analysis sight obstruction previously

428   modelled through 3D drawing software. As in this case, a faithful 3D reproduction of the guardrails

429   allows to obtain reliable results, with a minimum of error, compared to other methods that may be

430   more lacking.

431

432 *Implications*

433   Road designers should be aware of the impact of safety barriers on the *ASD* when considering the

434   installation of barriers. The presence of taller barriers, even though they can provide greater

435   containment levels, offer a reduced *ASD* value: in particular, worse visibility conditions detect in the

436   presence of the 3-waves barrier (H2 guardrail) compared to the N2 type. Given that the N2 barrier has

437   a lower height, it enabled greater *ASD*.

438   As the radius of the horizontal curve increases, it becomes more difficult to ensure *ASD* values

439   that allow safe braking manoeuvres. It is demonstrated in group 2 curves (those with larger radii of

440   curvature): as the radius increases, the difference between *SSD* and *ASD* increases too. This result is

441   consistent with expectations because of the link between curve radii and design speed values (the

442   higher the radius, the higher the design speed).

443   The worst sight conditions are certainly detected on right-hand curves. Comparing the curves,

444   the *ASD* values are greater in the left-hand bends than in the right-hand ones. Again, this is consistent

445   with expectations because of the dependence of *ASD* from the distance of the observer from the sight

446   obstruction (the smaller the distance, the smaller the *ASD*).

447   From different comparisons involving the vertical profile and the dimensions of the curves, it is

448   possible to see how the vertical profile affects the sight distance. Sag vertical curves increase *ASD*

449   values, while the presence of horizontal curves overlapped with crest vertical curves worsens the sight

450   conditions compared to a flat-grade terrain, especially in left-hand curves.

451

452   ***Limitations and future research needs***

453   This work is limited to the specific road type and the two guardrails considered. Other analysis should

454   be carried out with the aim of extend the results to different road and barrier typologies. Furthermore,

455   the position for the barrier in the roadside (or in the median) is another factor that affects the *ASD*

456   and that deserve specific analysis. The comparison between rigid and guardrails with different heights

457   and shapes will provide other insight on the effects of these road furniture on the *ASD*.

458   As future lines of research, the authors are working on a driving simulator study to check

459   whether the driver perceives and adapt their behavior to the different sight distance condition along

460   curves treated with the two different barriers.

461

462   **Data Availability Statement**

463   Some or all data, models, or code that support the findings of this study are available from the

464   corresponding author upon reasonable request.

465

466   **Acknowledgments**

472   **References**

473   Alcón Gil, P., De Santos-Berbel, C., and Castro, M. (2021). "Driver glare exposure with different vehicle

474   frontlighting systems." *Journal of Safety Research*, National Safety Council and Elsevier Ltd, 76,

475   228–237. https://doi.org/10.1016/j.jsr.2020.12.018

476   American Association of State Highway and Transportation Officials (AASHTO). (2011). *Roadside*

477   *Design Guide*. Washington, D.C.

478   American Association of State Highway and Transportation Officials (AASHTO). (2018). *A policy on*

479   *geometric design of highways and streets*. AASHTO, Washington, D.C.

480   Bassani, M., Grasso, N., and Piras, M. (2015). "3D GIS based evaluation of the available sight distance

481   to assess safety of urban roads." *International Archives of the Photogrammetry, Remote Sensing*

482   *and Spatial Information Sciences - ISPRS Archives*, 40, 137–143.

483   https://doi.org/10.5194/isprsarchives-XL-3-W3-137-2015

484   Bassani, M., Grasso, N., Piras, M., and Catani, L. (2016). "Estimating the available sight distance on

485   urban roads by integrating 3D maps and low-cost mobile mapping systems into a GIS numerical

486   computing environment." *Transportation Research Board 95th Annual Meeting*, Washington

487   D.C.

488   Bassani, M., Grasso, N., Piras, M., and Catani, L. (2019). "Estimating the available sight distance in the

489   urban environment by GIS and numerical computing codes." *ISPRS International Journal of Geo-*

490   *Information*, 8(2), 69. https://doi.org/10.3390/ijgi8020069

491   Campoy Ungria, J. M. (2015). "Nueva Metodología Para La Obtención De Distancias De Visibilidad

492   Disponibles En Carreteras Existentes Basada En Datos Lidar Terrestre." Universidad Politécnica

493   de Valencia, Valencia, Spain.

494   Castro, M., Anta, J. A., Iglesias, L., and Sánchez, J. A. (2014). "GIS-Based System for Sight Distance

495   Analysis of Highways." *ASCE Journal of Computing in Civil Engineering*, 28(3): 04014005.

496   https://doi.org/10.1061/(ASCE)CP.1943-5487.0000317

497   Castro, M., and De Santos-Berbel, C. (2015). "Spatial analysis of geometric design consistency and road

498   sight distance." *International Journal of Geographical Information Science*, 29(12), 2061–2074.

499   https://doi.org/10.1080/13658816.2015.1037304

500 Castro, M., De Santos-Berbel, C., and Iglesias, L. (2017). "A comprehensive methodology for the

501   analysis of highway sight distance." *Transport Infrastructure and Systems: Proceedings of the*

502   *AIIT*, 193–200, Rome, Italy: Associazione Italiana per l'Ingegneria del Traffico e dei Transporti.

503 Castro, M., Iglesias, L., Sánchez, J. Á., and Ambrosio, L. (2011). "Sight distance analysis of highways

504   using GIS tools." *Transportation Research Part C: Emerging Technologies*, 19(6), 997–1005.

505   https://doi.org/10.1016/j.trc.2011.05.012

506 Castro, M., López-Cuervo, S., Paréns-González, M., and de Santos-Berbel, C. (2016). "LIDAR-based

507   roadway and roadside modelling for sight distance studies." *Survey Review*, 48(350), 309–315.

508   https://doi.org/10.1179/1752270615Y.0000000037

509 De Santos-Berbel, C., Anta, J. A., Castro, M., and Iglesias, L. (2013). "Sight distance for road safety

510   analysis using GIS." *Esri Middle East Africa User Conference (EMEAUC)*, 1–9. Munich, Germany:

511   Esri Deutschland GmbH.

512 De Santos-Berbel, C., and Castro, M. (2018). "Three-dimensional virtual highway model for sight-

513   distance evaluation of highway underpasses." *Journal of Surveying Engineering*, 144(4),

514   05018003. https://doi.org/10.1061/(ASCE)SU.1943-5428.0000258

515 De Santos-Berbel, C., González-Gómez, K., Castro, M., and Anta, J. A. (2018). "Addressing sight-

516   distance-related safety effects of installing median barriers at horizontal curves of undivided

517   highways under a 3D approach." *5th International Conference on Road and Rail Infrastructure*

518   *(CETRA)*, 1067–1073. Zadar, Croatia: University of Zagreb.

519 Environmental Science Research Insitute (ESRI). (2008). *The multipatch geometry type*. Redlands,

520   California.

521 Environmental Science Research Institute (ESRI). (2021a). "Line of sight." Accessed May 28, 2021.

522   https://desktop.arcgis.com/en/arcmap/latest/tools/3d-analyst-toolbox/line-of-sight.htm

523 Environmental Science Research Institute (ESRI). (2021b). "Construct sight lines." Accessed May 28,

524   2021. https://desktop.arcgis.com/en/arcmap/latest/tools/3d-analyst-toolbox/construct-sight-

525   lines.htm

526 European Committee for Standardization (CEN). (2002). "ENV 1317-4. Road restraint systems. Part 4.

527   Performance classes, impact test acceptance criteria and test methods for terminals and

528   transitions of safety barriers."

529 European Committee for Standardization (CEN). (2011a). "EN 1317-1. Road restraint systems. Part 1:

530   Terminology and general criteria for test methods." Brussels, Belgium.

531 European Committee for Standardization (CEN). (2011b). "EN 1317-2. Road restraint systems. Part 2:

532   Performance classes, impact test acceptance criteria and test methods for safety barriers

533   including vehicle parapets."

534 European Committee for Standardization (CEN). (2012). "EN 1317-5. Road restraint systems. Part 5:

535   Product requirements and evaluation of conformity for vehicle restraint systems."

536 Gargoum, S. A., and El-Basyouny, K. (2020). "Analyzing the ability of crash-prone highways to handle

537   stochastically modelled driver demand for stopping sight distance." *Accident Analysis and*

538   *Prevention*, Elsevier, 136. https://doi.org/10.1016/j.aap.2019.105395

539 Gargoum, S. A., El-Basyouny, K., and Sabbagh, J. (2018). "Assessing Stopping and Passing Sight Distance

540   on Highways Using Mobile LiDAR Data." *Journal of Computing in Civil Engineering*, 32(4), 1–13.

541   https://doi.org/10.1061/(ASCE)CP.1943-5487.0000753

542 Ibrahim, S. E. B., and Sayed, T. (2011). "Developing safety performance functions incorporating

543   reliability-based risk measures." *Accident Analysis & Prevention*, Elsevier Ltd, 43(6), 2153–2159.

544   https://doi.org/10.1016/j.aap.2011.06.006

545 Iglesias, L., Castro, M., Pascual Gallego, V., and De Santos-Berbel, C. (2016). "Estimation of sight

546   distance on highways with overhanging elements." *3rd International Conference on Traffic and*

547   *Transport Engineering (ICTTE)*, 75–82. Belgrade, Serbia: City Net Scientific Research Center Ltd.

548 Iglesias, L., De Santos-Berbel, C., Pascual, V., and Castro, M. (2019). "Using small unmanned aerial

549   vehicle in 3D modeling of highways with tree-covered roadsides to estimate sight distance."

550   *Remote Sensing*, 11(2625), 1–13. https://doi.org/10.3390/rs11222625

551 Ismail, K. A., and Sayed, T. (2007). "New algorithm for calculating 3D available sight distance." *Journal*

552   *of Transportation Engineering*, 133(10), 572–581. https://doi.org/10.1061/(ASCE)0733-

553   947X(2007)133:10(572)

554 Jung, J., Olsen, M. J., Hurwitz, D. S., Kashani, A. G., and Buker, K. (2018). "3D virtual intersection sight

555   distance analysis using lidar data." *Transportation Research Part C: Emerging Technologies*,

556   Elsevier, 86(August 2017), 563–579. https://doi.org/10.1016/j.trc.2017.12.004

557 Khattak, A. J., and Shamayleh, H. (2005). "Highway safety assessment through geographic information

558   system-based data visualization." *Journal of Computing in Civil Engineering*, 19(4), 407–411.

559   https://doi.org/10.1061/(ASCE)0887-3801(2005)19:4(407)

560 Liu, C. (2013). "Exact sight distance determination on compound vertical and horizontal curves in the

561   presence of road barriers." *International Journal of Transportation Science and Technology*, 2(2),

562   159–166. https://doi.org/10.1260/2046-0430.2.2.159

563 Ma, Y., Zheng, Y., Cheng, J., and Easa, S. M. (2019). "Real-time visualization method for estimating 3D

564   highway sight distance using LiDAR data." *Journal of Transportation Engineering Part A: Systems*,

565   145(4): 04019006. https://doi.org/10.1061/JTEPBS.0000228

566 Ma, Y., Zheng, Y., Cheng, J., Guo, L., and Zhang, Y. (2018). "A novel real-time visualization algorithm

567   for computing three- dimensional sight distance." *Transportation Research Board Annual*

568   *Meeting*, (979).

569 Ministerio de Fomento. (2009). *Orden circular 28/2009 sobre criterios de aplicación de barreras de*

570   *seguridad metálicas*. España.

571 Ministerio de Fomento. (2014). *Orden Circular 35/2014 sobre criterios de aplicación de sistemas de*

572   *contención de vehículos*. España.

573 Ministerio de Fomento. (2016). *Instrucción de carreteras. Norma 3.1-IC*. España.

574 Ministero delle Infrastrutture e dei Trasporti. (2001). *Norme funzionali e geometriche per la*

575   *costruzione delle strade*. Rome, Italy.

576 *Ministero delle Infrastrutture e dei Trasporti. (2004). *Istruzioni tecniche per la progettazione,*

577 *l'omologazione e l'impiego dei dispositivi di ritenuta nelle costruzioni stradali*. Rome, Italy.

578 Montella, A. (2001). "Selection of roadside safety barrier containment level according to European

579 Union Standards." *Transportation Research Record*, (1743), 104–110.

580 https://doi.org/10.3141/1743-14

581 Papadimitriou, E., Mavromatis, S., and Psarianos, B. (2018). "Stopping sight distance adequacy

582 assessment on freeways: the case of left horizontal curves over crest vertical curves."

583 *Transportation Letters*, 10(5), 269–279. https://doi.org/10.1080/19427867.2016.1259759

584 Sarhan, M., and Hassan, Y. (2012). "Consideration of sight distance in placement of concrete barriers

585 on horizontal curves of roads." *Transportation Research Record*, (2301), 9–16.

586 https://doi.org/10.3141/2301-02

587 Shalkamy, A., El-Basyouny, K., and Xu, H. Y. (2020). "Voxel-based methodology for automated 3d sight

588 distance assessment on highways using mobile light detection and ranging data." *Transportation*

589 *Research Record*, 2674(5), 587–599. https://doi.org/10.1177/0361198120917376

590 Steinauer, B., and Mayer, G. (1999). "Sicherheitsdefizite in der Straßenplanung." *Straße und Autobahn*,

591 12(99), 655–662.

592 TOOL S.A. (2013). *Manual de instrucciones del programa CLIP sobre windows*. Madrid, Spain. TOOL,

593 S.A.

594 Trimble. (2013). "Extension Warehouse: CLF Shape Bender tool." Accessed December 6, 2020.

595 https://extensions.sketchup.com/extension/8a4d10ff-40f3-4885-b8ba-1dac2b941885/clf-

596 shape-bender

597 Wang, J., Lawson, G., and Shen, Y. (2014). "Advances in Engineering Software Automatic high-fidelity

598 3D road network modeling based on 2D GIS data." *Advances in Engineering Software*, Elsevier

599 Ltd, 76, 86–98. https://doi.org/10.1016 716/j.advengsoft.2014.06.005

600 Wang, J., Zhou, H., and Zhang, Y. (2017). "Improve sight distance at signalized ramp terminals of

601 partial-cloverleaf interchanges to deter wrong-way entries." *Journal of Transportation*

602   *Engineering*, 143(6), 04017017. https://doi.org/10.1061/JTEPBS.0000039